JOURNAL OF MATERIALS SCIENCE 28 (1993) 302–315

Review
Analysis of diffusion in lithium niobate

D. P. BIRNIE III
Department of Materials Science and Engineering, University of Arizona, Tucson, AZ 85721, USA

Possible diffusion paths in lithium niobate are discussed. The preferred path for diffusion is strongly influenced by the distribution of ions between the lithium and niobium sites; site swapping is important both for creating non-stoichiometric material and for impurity incorporation. Various literature reports of diffusion rates are surveyed for comparison with the possible diffusion mechanisms. Titanium (which is thought to substitute primarily for niobium) appears to diffuse more rapidly on the lithium sublattice in lithium-deficient samples.

1. Introduction

Lithium niobate is a promising non-linear optical material which finds application in optical waveguide switches, frequency conversion, and acoustic devices [1–3]. In many of these applications various diffusion processes are performed to obtain the desired structure or composition. This may be in- or out-diffusion to form optical waveguides or possible homogenization or alteration of the crystal's native stoichiometry. With the importance of diffusion in fabricating devices, it is useful to analyse the different diffusion mechanisms that are possible in this structure and to review the rates of diffusion for various elements.

The first section has four objectives: (1) to review the crystal structure, beause it provides the constraining environment for defect formation and diffusion, (2) to review the current understanding of non-stoichiometry and defect incorporation, (3) to provide a quantitative framework for describing the interrelationship between different defect concentrations, and (4) to develop diffusion equations that incorporate non-stoichiometry and site swapping.

In the second section, the various diffusion data are reviewed and analysed in the light of the diffusion equations that are developed. Finally, general conclusions are made regarding diffusion in this structure.

2. Defects and diffusion

The crystal structure of the ferroelectric (FE) phase of lithium niobate is a derivative of the corundum structure, belonging to the space group R3c. It has a hexagonal-close-packed oxygen lattice with two-thirds of the octahedral interstices filled with cations. The filling of the octahedral sites by the lithium and niobium is performed in an ordered arrangement such that the crystal acquires a net polarity [4–6]. Looking along the crystallographic c-axis, this cation arrangement is always in the sequence lithium, niobium, vacancy, lithium, niobium, vacancy, etc. This cation arrangement is reversed for the opposite polarity FE domain structure. These columns of octahedral cation sites are packed together such that in the basal plane every lithium ion has three nearby niobium ions and three nearby structural vacancies; each niobium has three lithiums and three vacancies; and, each vacancy has three each of lithium and niobium. Fig. 1 illustrates the arrangement of cations in octahedral sites in the basal plane.

The above description of lithium niobate is applicable only up to the Curie temperature, T_c, where the structure transforms to a paraelectric structure [6–10], with space group $R\bar{3}c$. Because the vast majority of diffusion processing is performed in the low-temperature phase, no discussion of diffusion in the paraelectric phase will be attempted.

This ideal crystal structure has a stoichiometry of "$LiNbO_3$". However, most commercially available crystals have a composition that is significantly niobium-rich [11–14]. Careful X-ray diffraction structure analysis comparing congruent and stoichiometric composition crystals has determined that at room temperature the niobium excess is accommodated by niobium atoms sitting on lithium sites with an appropriate number of niobium vacancies for charge balance [14]. No significant number of oxygen vacancies were found which has been confirmed by others using density measurements [11, 15].

This defect structure at room temperature may not be entirely retained at the high temperatures required for diffusion. It has been proposed that at high temperatures the main charge balance is niobium atoms at lithium sites with lithium vacancies offering charge balance [16–20]. On cooling, this can transform to the niobium vacancy charge balance description as above; normal site niobiums jump into the lithium vacancies, creating defect pairs of $(Nb_{Li}V_{Nb})'$ [18–20]. X-ray diffraction cannot distinguish this mechanism from the defect structure originally proposed by Abrahams and Marsh [14].

The above defect studies and explanations have given the following four defects as possible contributors to nonstoichiometry: $Nb_{Li}^{\cdots}$, V_{Li}', $V_{Nb}^{''''}$, $(Nb_{Li}V_{Nb})'$ using Kröger–Vink notation [21], where the subscript

0022–2461

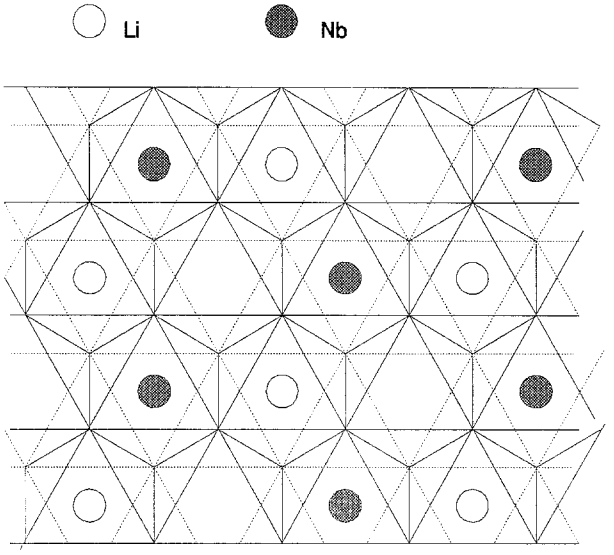

Figure 1 The arrangement of cations in the basal plane of lithium niobate. The surrounding oxygen sublattice is represented by lines connecting nearest neighbour oxygen centres; the two layers of oxygen atoms sandwich the cations into octahedral sites.

TABLE I Applicability of various charge neutrality conditions in different temperature ranges.

	Low temperature	High temperature
$4[Nb_{Li}^{\cdots\cdot}] = [V_{Li}']$	*Disallowed* (Abrahams and Marsh diffraction study)	*Preferred* (Very rapid lithium diffusion)
$4[Nb_{Li}^{\cdots\cdot}] = [(Nb_{Li}V_{Nb})']$	*Preferred* (Coulombic attraction of point defects during cooling)	*Possible* (Likely as transition stage from low to high temperature)
$4[Nb_{Li}^{\cdots\cdot}] = 5[V_{Nb}^{\prime\prime\prime\prime\prime}]$	*Not Preferred* (High charge of separate point defects)	*Not Likely* (Diffusion of lithium much more rapid than niobium)

represents the defect location and the superscript denotes the relative defect charge ($'''' = -5$, $\cdots = +4$, etc.).

To ensure overall charge neutrality, the concentrations of positive and negative charge concentration must balance. This defines the charge neutrality equation:

$$4[Nb_{Li}^{\cdots\cdot}] = [V_{Li}'] + [(Nb_{Li}V_{Nb})'] + 5[V_{Nb}^{\prime\prime\prime\prime\prime}] \quad (1)$$

where brackets indicate that concentrations of the respective defects are being summed. This can be simplified in one of three ways, depending on which negative defect dominates. Table I helps to discriminate between these possible choices for cation vacancy location. Each of the three possible charge neutrality conditions (or Brouwer approximations) is listed as a separate row, and low- and high-temperature behaviour are given as columns. Each table entry discusses the likelihood of this reaction dominating at a given temperature. The most plausible sequence that spans the tempeature range is having the defect clusters dominate at low temperatures with a gradual transition toward primarily free lithium vacancies at high temperature.

This defect state can be described with the following set of equations. The cluster defects establish an equilibrium concentration through reaction between lithium vacancies and a neighbouring normal-site niobium atom

$$(Nb_{Li}V_{Nb})' \rightarrow V_{Li}' + Nb_{Nb}^{x} \quad (2)$$

This has an equilibrium constant (dependent only on temperature) of

$$K_1 = \frac{[V_{Li}']}{[(Nb_{Li}V_{Nb})']} \quad (3)$$

The transition from "low-temperature" to "high-temperature" behaviour is governed by this equilibrium constant. We have no direct information on the value of either the enthalpy or the entropy for this reaction, but the "low-temperature" conditions apply whenever $K_1 \ll 1$ and "high-temperature" conditions apply whenever $K_1 \gg 1$. This transition could easily happen when going from room temperature to the common diffusion temperatures in the range of 1000 °C. In later discussions, the labels "low" and "high" will implicitly refer to temperature ranges where K_1 satisfies one of these inequalities. It is recognized that the energetics of Reaction 2 may prevent the low-to-high transition from ever happening. Then, all diffusion would be governed by the few vacancies that escaped from the clusters. As we will see below (where both high and low temperature cases are developed) the composition dependencies of the diffusion rates are not dependent on this transition; instead this transition mainly influences the value of the activation energy found for diffusion.

The cluster defects may also dissociate to form niobium vacancies that will be required for diffusion on the niobium sublattice. These niobium vacancies are important for diffusion, even if they are small in number

$$(Nb_{Li}V_{Nb})' \rightarrow V_{Nb}^{\prime\prime\prime\prime\prime} + Nb_{Li}^{\cdots\cdot} \quad (4)$$

This has an equilibrium constant of

$$K_2 = \frac{[V_{Nb}^{\prime\prime\prime\prime\prime}]\,[Nb_{Li}^{\cdots\cdot}]}{[(Nb_{Li}V_{Nb})']} \quad (5)$$

Because of the conservation of cation vacancies found in Reactions 2 and 4, the overall stoichiometry of the crystal can be defined by one constant, C_V, the total cation vacancy concentration

$$[V_{Li}'] + [Nb_{Li}V_{Nb})'] = C_V \quad (6)$$

This parameter has been used previously when describing the composition dependence of the ferroelectric phase transition [10, 22].

As discussed above, at low temperatures the majority of cation vacancies are likely to be bound in clusters

$$[(Nb_{Li}V_{Nb})'] \simeq C_V \quad (7)$$

For this case, the minority vacancy concentrations can be found using Equation 3

$$[V'_{Li}] = C_V K_1 \quad (8)$$

And, using Equations 1 and 5, the minority niobium vacancy concentration is

$$[V''''''_{Nb}] = 4K_2 \quad (9)$$

If temperatures become high enough (or the energy for cluster transformation is low enough) then at high temperatures the majority of cation vacancies will exist as free lithium vacancies

$$[V'_{Li}] \simeq C_V \quad (10)$$

Then using Equation 3 the clustered vacancy concentration will be

$$[(Nb_{Li}V_{Nb})'] = \frac{C_V}{K_1} \quad (11)$$

and the minority niobium vacancy concentration will be

$$[V''''''_{Nb}] = \frac{4K_2}{K_1} \quad (12)$$

These defect chemical reactions with their equilibrium constants form a simple basis for analysing vacancy-type diffusion rates and their dependence on crystal stoichiometry.

To summarize the defect chemistry, it is believed that plentiful lithium vacancies are available for diffusion at high temperature (possibly depending on their escape rate from cluster defects). Mobile niobium vacancies become available by simple dissociation of the cluster defects, but this will not dominate the charge balance.

Other types of defects certainly occur, but in relatively low concentrations that will depend on the temperature and the activation energy for their creation. Thus, although previous studies have resorted to oxygen vacancies to explain oxidation and reduction behaviour [23, 24], the same behaviour would occur for a reduction model based entirely on cation sublattice defects [18–20, 25]. Therefore, no oxygen vacancies are included in the present analysis.

The location of impurity substitution is important in understanding their rate of diffusion. Very little conclusive work exists on impurity substitution. Many of the studies simply give the local site symmetry (which in other crystal structures is often enough to pin-point their site). In the lithium niobate structure all of the likely locations for the impurities have octahedral symmetry, so many spectroscopic techniques are insufficient to locate the impurity site.

Because of the similarity between possible sites, impurity site substitution locations cannot be viewed as purely limited to one site. In fact, there is much evidence that impurities are distributed between more than one site, although probably at different concentration levels [26–33]. In fact, one study has monitored the temperature dependence of the hafnium distribution between two different sites [33]. This is compatible with the behaviour of the niobium atoms as described above; site swapping must be incorporated into any model that thoroughly describes the diffusion of impurities.

Site swapping will become progressively more important at high diffusion temperatures where entropy factors start to overtake enthalpy contributions. It should be noted that other crystal structures, with multiple cation sites, also exhibit extensive cation disordering and site swapping. This is especially prevalent in the spinel structure where the swapping is between octahedral and tetrahedral sites [34]. Thus, in lithium niobate (with two octahedral sites having much closer size) it might be expected that site swapping would also be easy.

A chemical reaction that represents the equilibrium condition for impurities that become distributed between the two likely sites would be

$$I_{Li} + V_{Nb} \rightarrow I_{Nb} + V_{Li} \quad (13)$$

Note that the defect charges have been omitted to make this general to all valence impurities. Whatever the valence of the impurity, no oxidation or reduction occurs, so charge will be conserved. The equilibrium constant for this process is

$$K_3 = \frac{[I_{Nb}]\,[V_{Li}]}{[I_{Li}]\,[V_{Nb}]} \quad (14)$$

The above equilibrium constants (Equations 3, 5 and 14) define the defect chemistry for a doped, non-stoichiometric crystal of lithium niobate, and will be used below in the description of the various diffusion paths.

The above summary of the crystal structure and defect chemistry in lithium niobate can help us understand diffusion mechanisms; diffusion occurs through the motion of point defects, including lithium vacancies and niobium vacancies. Niobium antisite defects and defect clusters may also be important. Because of the large number of vacancies present, this discussion will be confined to diffusion occurring via vacancy mechanisms. However, because significant rates of site swapping are known to occur in this crystal, this effect will also be included.

Fig. 2 illustrates the likely migration path for a substitutional impurity in lithium niobate. Note that because of the lithium and niobium arrangement, the two sublattices are self-similar; this basal-plane cut shows that for either sublattice the diffusing atom can jump into a vacancy on the same sublattice by following a path that winds through the normally vacant octahedral site in the structure. At an atomic level, this migration path is far from direct. It starts at the normal site, pushes through a triangle of oxygen atoms that define the face of the normal site octahedron, this puts the atom in a tetrahedral site (a), it must then push through another oxygen triangle (different size) to reach the structural vacancy (b), then it again pushes oxygens apart to reach another tetrahedral site

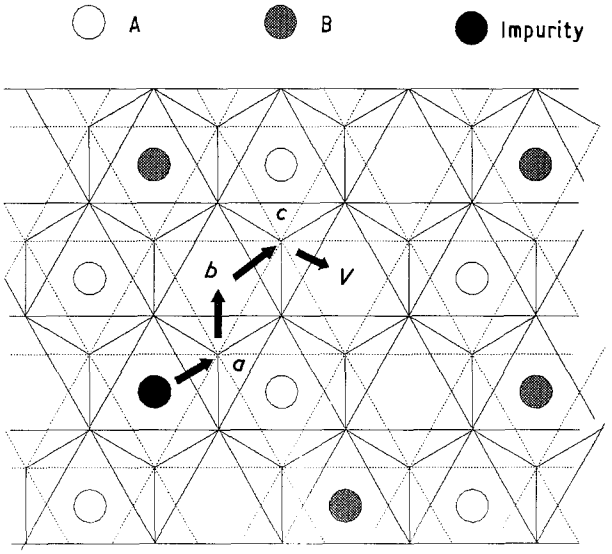

Figure 2 Basal plane arrangement showing the migration path for a substitutional impurity. Because of the symmetric similarity of the lithium and niobium sublattices this migration path serves to explain motion for cations on either sublattice. Four partial jumps are represented by the short arrows. These correspond to jumps where the impurity pushes through oxygen triangles when moving between octahedral and tetrahedral sites.

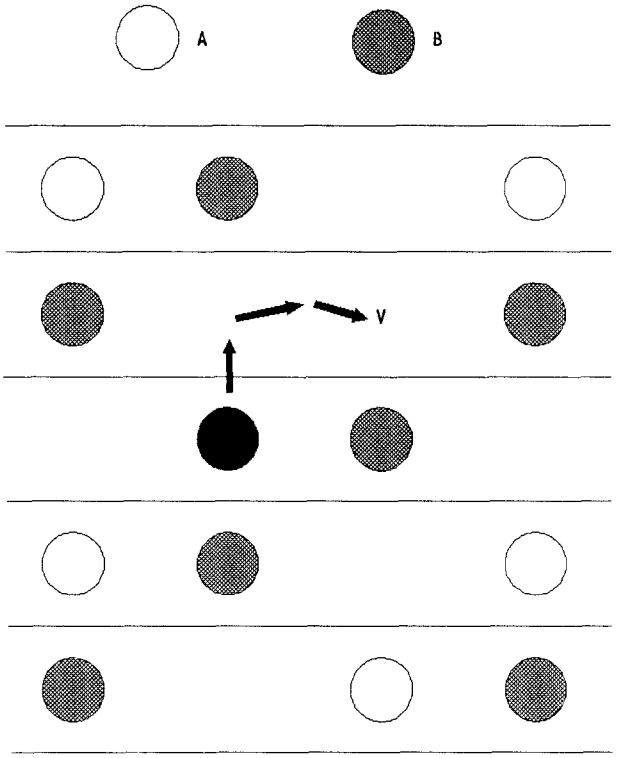

Figure 3 A cut vertical to the basal plane illustrating the likely impurity migration that results in diffusion parallel to the *c*-axis. The horizontal solid lines represent the oxygen close-packed-planes that sandwich the cations. Again, because of the site similarity, dark and light circles represent either lithium or niobium, and the black circle is any substitutional impurity. The second and third jumps in this path are identical to the last two jumps in the basal plane migraton sequence shown in Fig. 2.

(c) and finally reaches the vacant cation site by pushing a fourth oxygen triangle apart. These triangular oxygen arrangements are important for the diffusion; they define the locations of largest strain (and therefore the migration enthalpy). Beause the first and second oxygen triangles along the route are different in size, only one of them will limit the rate of migration. But the requirement for two jumps of this type will lower the overall migration frequency by a factor of 2 [35]; the main limitation to the migration rate will be the peak energy required to push the diffusing atom through.

Fig. 3 shows a vertical cross-section of the lattice to illustrate the migration path in the other crystallographic direction. Again, impurities substituting on to either site must follow a topologically similar route. However, the route in this direction passes from the starting site, through an oxygen triangle directly into the normally vacant octahedral site, and then laterally through two O-triangles and the tetrahedral site (exactly the same as the second half of the migration path found for diffusion in the basal plane, described above).

All of the diffusion paths, either in the basal plane or along the *c*-axis, must pass through similar oxygen constrictions. Therefore, as a first approximation, the diffusion will be isotropic in this structure. Only if the direct octahedral-site to normally-vacant octahedral-site is significantly harder will the diffusion rates be anisotropic (and then it could only be slower parallel to the *c*-axis).

Diffusion on either sublattice requires a vacancy at a site close to the impurity substitution site. Thus, the motion of an atom on a lithium site requires a free lithium vacancy (regardless of temperature) and the motion of an atom on a niobium site requires a free niobium vacancy. If the impurity atom is partially distributed between the two types of site, then the cumulative measured diffusion rate will be the sum of the contributions by these two routes

$$D_I = f_{Li}[V'_{Li}] \exp\left(-\frac{Q_{Li}}{RT}\right) + f_{Nb}[V''''_{Nb}] \exp\left(-\frac{Q_{Nb}}{RT}\right) \quad (15)$$

where f_i denotes the fraction of impurities on either the lithium or niobium sites. These fractions range between 0 and 1, and will depend on the equilibrium constants that defined the defect chemistry. For the simplicity of further calculations, it will be assumed that any given impurity prefers one particular site, but swaps occasionally on to the other sublattice. Therefore, either f_{Li} or f_{Nb} will be approximately 1, while the fraction for the non-preferred site will be much smaller.

For an atom that prefers the lithium site it is assumed that no significant amount of migration occurs through niobium vacancies. Then simplifying Equation 15 using either the low- or high-temperature solutions for the lithium vacancy concentration Equations 8 or 10) gives:

low T temperature

$$D_I = C_V K_1 \exp\left(-\frac{Q_{Li}}{RT}\right) \quad (16)$$

and high T temperature

$$D_I = C_V \exp\left(-\frac{Q_{Li}}{RT}\right) \quad (17)$$

Note that, for both low- and high-temperature models for cluster action, the impurity diffusivity will vary linearly with the deviation from stoichiometry (as measured by C_V, the total cation vacancy fraction). The only difference is the factor of K_1; this will only influence the activation energy measured. However, we are seldom able to differentiate partial contributions to the activation energies; the primary utility of these equations is their composition dependence.

Atoms that substitute entirely for niobium will diffuse slowly, moving only when free niobium vacancies are available. However, significant diffusive flows could occur through some minority fraction that swaps, even temporarily, on to the lithium sublattice, and then migrate via lithium vacancies. With the greater concentration of mobile lithium vacancies, this flux could dominate. The total flux will have contributions from both lithium and niobium vacancies. In this case the fractional occupation by the impurity on the lithium site (given $f_{Nb} \approx 1$) will be

$$f_{Li} = \frac{C_V K_1}{4 K_2 K_3} \quad (18)$$

Again we use Equation 15 and evaluate it in both the low- and high-temperature cases:
low temperature

$$D_I = \frac{C_V^2 K_1^2}{4 K_2 K_3} \exp\left(-\frac{Q_{Li}}{RT}\right) + 4 K_2 \exp\left(-\frac{Q_{Nb}}{RT}\right) \quad (19)$$

high temperature

$$D_I = \frac{C_V^2 K_1}{4 K_2 K_3} \exp\left(-\frac{Q_{Li}}{RT}\right) + 4 \frac{K_2}{K_1} \exp\left(-\frac{Q_{Nb}}{RT}\right) \quad (20)$$

Notice again that the low- and high-temperature cases have identical composition dependencies, and that the two components to each equation have different composition dependencies. Diffusion that occurs via lithium vacancies (and the minority fraction of the substituted impurity) will vary as C_V^2, while diffusion that occurs via the niobium vacancies will be independent of composition. This shows that there could easily be a transition between diffusion mechanisms for samples with different stoichiometry; specifically, the lithium vacancy contribution will diminish drastically for samples that are more stoichiometric.

The self-diffusion behaviour can also be analysed using these same equations. For lithium self-diffusion, Equation 16 or 17 would apply. For niobium self-diffusion Equation 19 or 20 would be used. However, they become simplified because the site-swapping equation used for impurities no longer applies. The site-swapping equilibrium constant, K_3, must be replaced by the ratio of K_1/K_2. This still leaves the same concentration dependencies found before. The niobium self-diffusion could be somewhat more complicated. In addition to the simple lithium vacancy or simple niobium vacancy mechanisms used in developing Equations 19 and 20, a third mechanism becomes possible [36, 37]. This third mechanism is analogous to an interstitialcy mechanism where the niobium antisite defect displaces a normal site niobium, domino fashion, into the lithium vacancy beyond. This path gives identical composition dependence as found above, and could only possibly lower the value of the activation energy for diffusion. However, given the similarity in jump paths required, this is not expected. Therefore, the simple analysis used for impurity atoms should be applied to niobium self-diffusion as well.

3. Analysis of diffusion data

The previous section has developed equations that show the specific concentration dependencies for vacancy diffusion of impurities, at low- or high-temperature, and depending on their preferred site of substitution. In this section a review of the observed diffusion rates in lithium niobate is presented. The diffusion data are separated into some related groups and tables of diffusion data are presented. As the data are presented, different salient features are highlighted. They are discussed with particular attention to diffusion anisotropy and to composition dependencies that have been observed.

The majority of diffusion experiments actually measure the chemical diffusion coefficient. For these experiments a concentration gradient is applied to the sample and the rate of mass transport is quantified; this is different from tracer diffusivities that are performed with only a gradient in those atoms that have been isotopically labelled. The chemical diffusion coefficient is always more difficult to interpret because it combines the effects of host atoms that are diffusing in the opposite direction (and possibly of charge-balancing defects diffusing together with the impurities, or ambi-polar diffusion) [38, 39].

In addition, many of the diffusion rates have been inferred from optical index changes upon formation of in-diffused optical waveguides. This retrieves the diffusion data based on the assumption that the refractive index changes linearly with concentration of impurity atom. This relationship has been measured and is reasonably linear over a range of concentrations [40–44]. However, the various reports of differences between X-cut and Y-cut diffusion rates are anomalous; diffusion is a second rank tensor which should be isotropic in the basal plane of a hexagonal system. However, because the in-diffusion is often accompanied by lattice mismatch, near surface strains may account for some of the index change on in-diffusion [43, 45]; this higher-order tensor effect could easily account for the difference.

A general effort has been made to plot published data points in the figures here. But for the sake of figure clarity, some data are presented only as the reported linear regression fit. Readers are urged to make reference to the original literature.

Fig. 4 shows a master plot of diffusion data in lithium niobate. This is presented without significant discussion because all data shown here are included in later groupings. This figure simply serves to emphasize

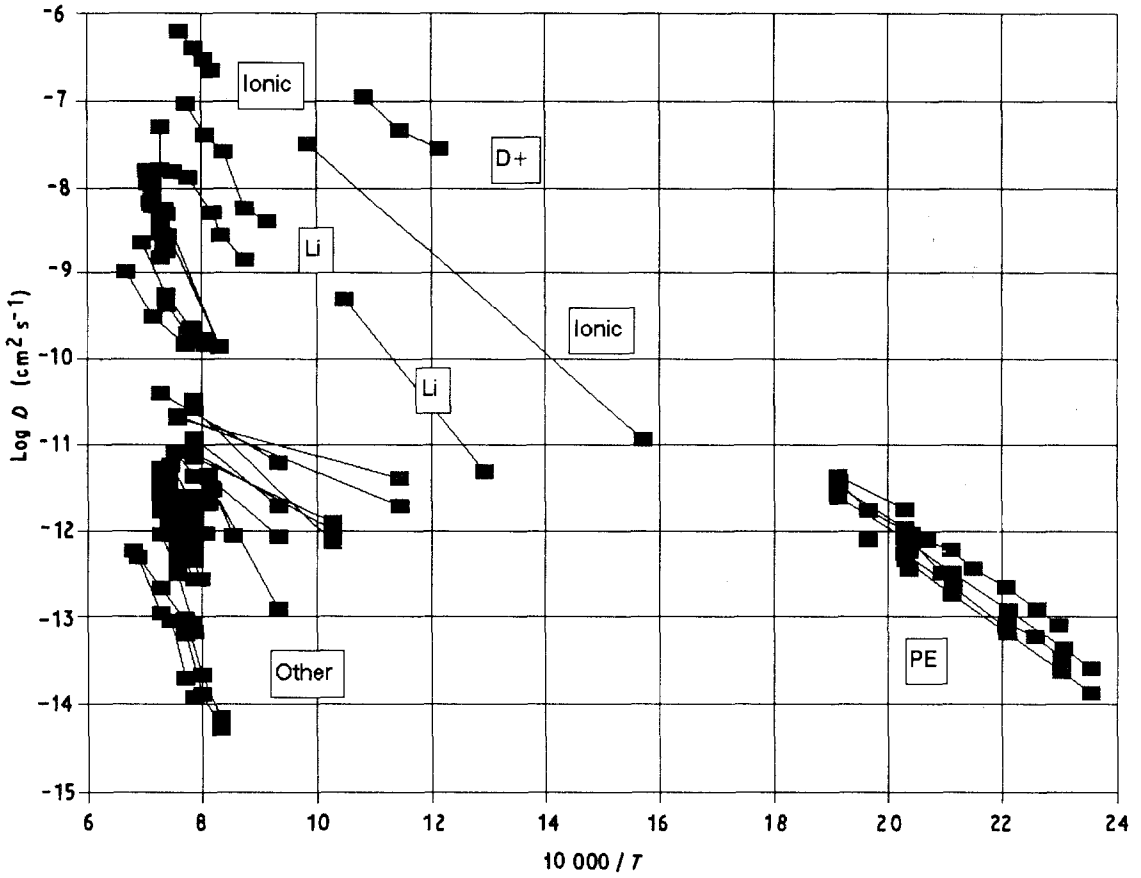

Figure 4 Accumulated diffusion data in lithium niobate serve to emphasize the wide range of diffusion rates, spanning eight decades. All groupings are more specifically treated in later tables and figures. "PE" identifies low-temperature proton exchange rates. Some rapid diffusers are deuterium (and hydrogen), ionic carriers, and lithium ions. Other species move significantly more slowly.

the rather wide range of diffusion rates that different atomic species exhibit; the data span over eight orders of magnitude! Labels indicate various groups of data: "PE" refers to data obtained from proton exchange studies of waveguide formation, "Ionic" refers to data obtained from conductivity data. "D + " is for the motion of deuterium, and "Li" is for lithium tracer and NMR line-broadening kinetics rates. All other species move at considerably slower rates; much higher temperatures have been required to form waveguides of appreciable depths with these other ions.

Fig. 5 groups all data for diffusion of hydrogen, deuterium, lithium and other alkali ions. Table II presents all hydrogen and deuterium diffusion information. For each literature citation the range of temperatures used in the study is given as well as the activation energy, E_a(eV), and the diffusion pre-exponential factor, D_0 ($cm^2\,s^{-1}$). When data are available for only one temperature, no activation energy can be derived; in these cases, the absolute diffusion rate is given in the D_0 column, and E_a remains blank. The "comments" column gives the diffusion direction or other information that may be pertinent to the discussion. This format for presenting the data will also apply to the remainder of the tables.

For hydrogen (and deuterium) the majority of data have been obtained from proton exchange (PE) studies which must be considered to be chemical diffusion studies that might be rate limited by the motion of lithium rather than hydrogen. However, this cannot be ascertained. In general, the studies show an activation energy of around 0.9 eV with relatively isotropic diffusion rate. There is a slightly slower diffusion rate in the Z-direction (along the crystallographic c-axis). Deuterium diffuses slightly slower than hydrogen, in conformance with expectations based on the isotope mass difference. Also the PE rate is reduced by having higher concentrations of lithium in the benzoic acid melts. This is consistent with the PE process occurring by a chemical diffusion process that involves removal of lithium from the surface at the same time that protons are being introduced; the larger concentration of lithium in the melt then causes a smaller driving force to be applied to lithium removal, even if the proton gradient is nearly the same. This slows the overall PE rate. The observation that titanium incorporation slows PE [52] may also be occurring through this effect; the titanium was introduced by in-diffusion which will also be lowering the lithium content and thus the concentration gradient near the surface. This reduces the PE rate. Because the titanium was added by in-diffusion, it is probably not possible to make defect chemistry arguments (with implied local equilibrium) about the relative diffusion rate.

Fig. 5 also emphasizes the ion-size effect on diffusion rate. Hydrogen and deuterium both exhibit extremely rapid diffusion rates, while the larger alkali ions move progressively slower with increasing size. The lithium and alkali ion-diffusion rates are presented in Table III.

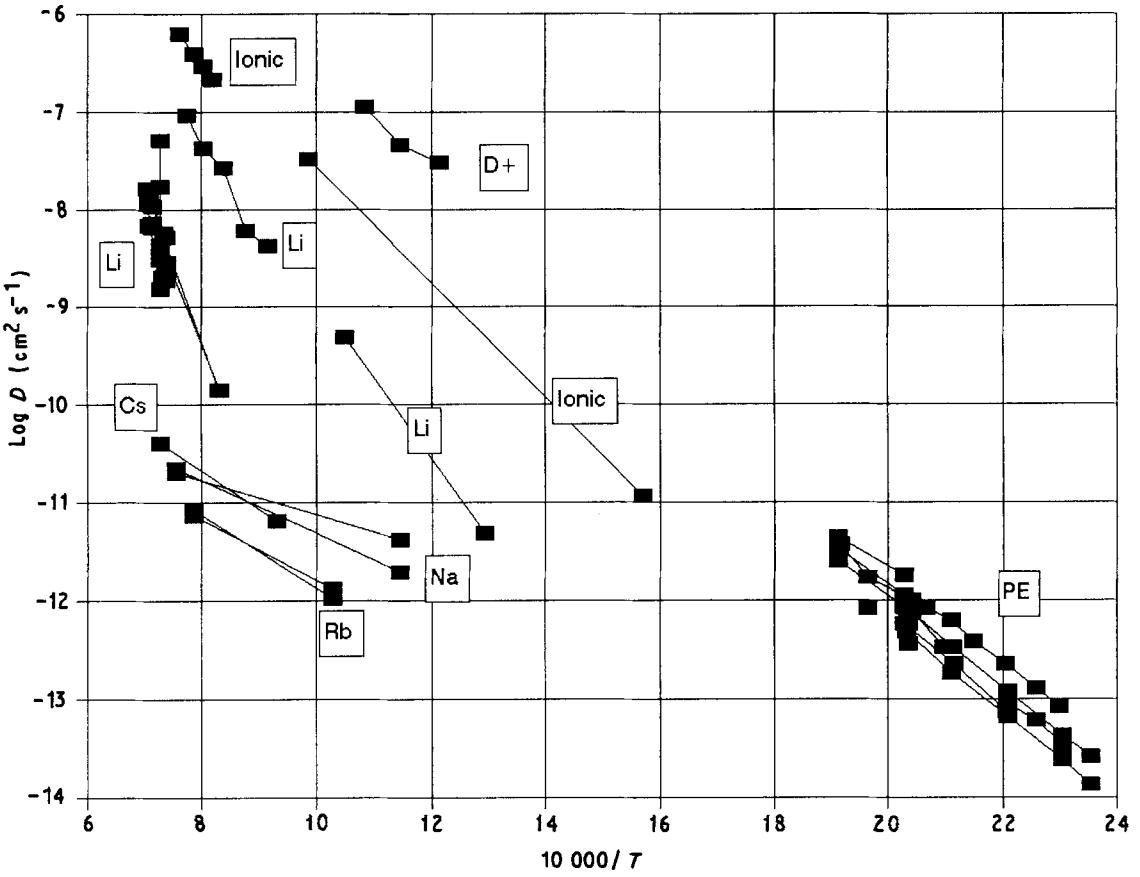

Figure 5 Diffusion data for hydrogen, lithium, and other alkali ions. Ionic conduction data are presented assuming conduction via the concentration of cation vacancies that would be present in congruent lithium niobate.

TABLE II Hydrogen diffusion in lithium niobate

Atom	Method	$T(K)$	E_a	D_o^a ($cm^2 s^{-1}$)	Comments	Reference
H +	PE	425–492	0.94	2.1×10^{-3}	Z	[46]
		425–492	0.92	2.3×10^{-3}	X	
		434–453	0.86	3.5×10^{-4}	Y	
					$D_x > D_y > D_z$	
D +	PE	509	–	8.1×10^{-13}	Z	[40]
D +	Vapour exchange	823–923	0.87	5.4×10^{-3}	Z Isotropic	[47]
H +	PE	491	–	7.4×10^{-13}	X-cut in air	[48]
H +	PE	491	–	5.9×10^{-13}	X-cut in argon	
D +	PE	491	–	3.6×10^{-13}	X-cut in argon	
					$D_D < D_H$	
H +	PE	490–522	0.92	2.5×10^{-3}	X	[49]
					$D_z < D_x$	
H +	PE	453–493	0.98	6.1×10^{-3}	Z	[50]
H +	PE	434–484	0.87	1.0×10^{-3}	X	[51]
H +	PE	493–523	0.67	1.2×10^{-5}	Y (Pure)	[52]
		493–523	0.81	2.3×10^{-4}	Y (Some titanium)	
		493–523	0.81	1.7×10^{-4}	Y (More titanium)	
					Titanium lowers PE	
H +	PE	477–490	1.31	2.6×10^{1}	X	[53]
H +	PE	–	–	–	Lithium in benzoic acid melt lowers PE rate	[54]

[a] When diffusion data are available for only one temperature, only the absolute rate is presented in this column, otherwise this column does present D_o, the pre-exponential constant.

TABLE III Alkali ion diffusion in lithium niobate

Type	Method	T(K)	E_a	D_0(cm^2 s^{-1})	Comments	Reference
Li	OD	1203–1398	2.96	3.3×10^2	Z	[55]
		1203–1398	3.24	5.0×10^3	$\perp Z$	
Li	OD	1373	–	1.5×10^{-9}	D_Z	[56]
		1373	–	4.2×10^{-9}	D_Y	
Li	Ionic cond.	1223–1316	1.55	5.1×10^{-1}	Isotropic	[57]
Li	NMR	773–953	1.62	1.8×10^{-1}	NMR line broadening	[58]
Li	OD	1356–1416	3.24	5.7×10^3	49.9% Li	[59]
		1353–1407	2.83	9.5×10^1	48.8% Li	
		1354–1415	[a]	[a]	48.5% Li	
					$D_{\text{Li-rich}} > D_{\text{Li-poor}}$	
					$D_{\text{Surface}} > D_{\text{Bulk}}$	
Li	Tracer	1093–1293	1.98	4.7×10^0	–	[60]
Li	Ionic cond.	636–1013	1.17	2.1×10^{-2}	–	[61]
Li	Thermo-gravimetry	1373	–	$1–8 \times 10^{-8}$	Faster as lithium removed	[62]
Li	In-diffusion	1373	–	$3–50 \times 10^{-9}$	Faster near stoichiometry	[63]
Na	Tracer	873–1323	0.36	4.6×10^{-10}	Z	[64]
		873–1323	0.54	2.5×10^{-9}	Y	
Rb	Tracer	973–1273	0.62	2.0×10^{-9}	Z	[64]
		973–1273	0.73	6.3×10^{-9}	Y	
Cs	Tracer	1073–1373	0.79	3.2×10^{-8}		[64]

[a] Not calculated because authors attribute highest temperature data to the paraelectric phase rather than the ferroelectric phase.

The lithium diffusion data from all techniques exhibit rather isotropic diffusion rates. In contrast to the hydrogen diffusion data that are primarily a result of proton exchange studies, there have been many techniques applied to measuring lithium motion, including isotropic tracer, conductivity, NMR line-broadening, out-diffused waveguides, and thermogravimetry. The diffusivities derived from conductivity studies have been calculated and plotted here based on the assumption that lithium vacancies are responsible for the electrical current. The congruent crystal composition was chosen for estimating the ionic carrier concentration. The absolute magnitude of these conductivity-based diffusivities will depend on this choice; the diffusivities will be larger if the carrier concentration is lower (i.e. if these studies came from more stoichiometric crystals, or if other defects were rate limiting).

The activation energy of lithium diffusion is in the region of 1.5 eV, as found from tracer diffusion and ionic conduction studies. The lithium diffusion data that have resulted from lithium out-diffusion (OD) kinetics are uniformly slower than those measured by tracer or other non-gradient techniques. This is interesting because it indicates that the out-diffusion process requires the motion of some other, slower, species at the same time that lithium is being removed from the surface. Thus some mixture of lithium, niobium, and/or oxygen diffusion is really being represented by the lithium out-diffusion data; this results in their uniformly higher activation energies.

The concentration dependence of lithium in-diffusion has been investigated at 1100 °C [63].

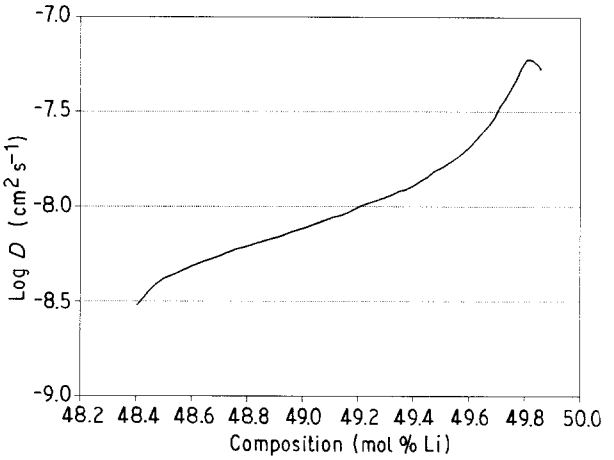

Figure 6 Concentration dependence of lithium in-diffusion as determined by a Boltzmann–Matano analysis (from [63]).

Fig. 6 shows the resulting chemical diffusion coefficient as determined by a careful Boltzmann–Matano analysis. Interestingly, the diffusion is more rapid as the composition becomes more lithium rich. This suggested that lithium interstitials were important [63]. The possibility of lithium interstitials is certainly compatible with the proposed phase transformation behaviour [9, 10]; however, the rate-controlling species for interdiffusion is not known, as mentioned above. Because there is little evidence for other elements dissolving interstitially, the present analysis will focus on diffusion via the vacancy mechanism as described earlier.

Other reports of possible oncentration effects on lithium diffusion exist [59, 62]. One shows that lithium out-diffusion is faster in material that has higher lithium content [59]. However, the same research also comments that lithium diffusion is faster in the surface region (which would naturally be lower in lithium content). This behaviour is difficult to understand within the framework presented here. Thermogravimetry also shows some limited concentration dependence of the chemical diffusivity [62], with diffusion being faster in lithium-poor samples. No uniform picture of lithium diffusion or its composition dependence can be distinguished.

The comparison between lithium diffusion and other alkali ions shows that the larger ions all diffuse more slowly (as we would naturally expect), but that the calculated activation energies are surprisingly low for these ions. It is possible that scatter in the experimental data prevented accurate determination of these activation energies. Also, we might expect larger differences between sodium, rubidium and caesium rates; instead these are rather similar in rate. Again, these are tracer measurements of the chemical diffusivity; these may also be limited by the diffusion of other species.

One set of lithium diffusion data are included again in Fig. 7 for comparison with the niobium and oxygen diffusion data. These diffusivity parameters are listed in Table IV. As we might expect, lithium diffuses fastest. Niobium and oxygen seem to diffuse with similar rates; interdiffusion studies between $LiNbO_3$ and $LiTaO_3$ exhibit significantly slower rates, possibly due to slower diffusion by the tantalum ions. The slow rate for oxygen motion is important in the light of rather rapid oxidation and reduction kinetics; samples are observed to darken or become black rapidly when reduced at high temperatures [23, 67]. This occurs much faster than would be possible if massive oxygen transport were required. Instead, the coloration can be occurring through cation diffusion [18–20, 24, 25]. This could give oxidation and reduction that would influence the electrical conduction behaviour without actually having long-distance oxygen motion.

Other cation diffusion data are presented graphically in Fig. 8 and numerically in Table V. The titanium diffusion rates are presented as a shaded region for comparison, and will be given explicitly in the following figure and table. Both magnesium and erbium diffusion data have been collected both parallel and perpendicular to the c-axis and both species

TABLE IV Self diffusion in lithium niobate

Type	Method	T (K)	E_a	D_0(cm^2 s^{-1})	Comments	Reference
Li	Tracer	1093–1293	1.98	4.7×10^{0}	–	[60]
Nb	Tracer	1073–1273	1.07	2.0×10^{-7}	–	[64]
Nb–Ta	Inter-diffusion	1273–1473	1.73	5.0×10^{-7}	–	[65]
Nb–Ta	Inter-diffusion	1373–1458	3.05	1.8×10^{-2}	$^{\perp}Z$	[66]
O	Tracer	973–1273	1.27	3.0×10^{-6}	Isotropic	[24]

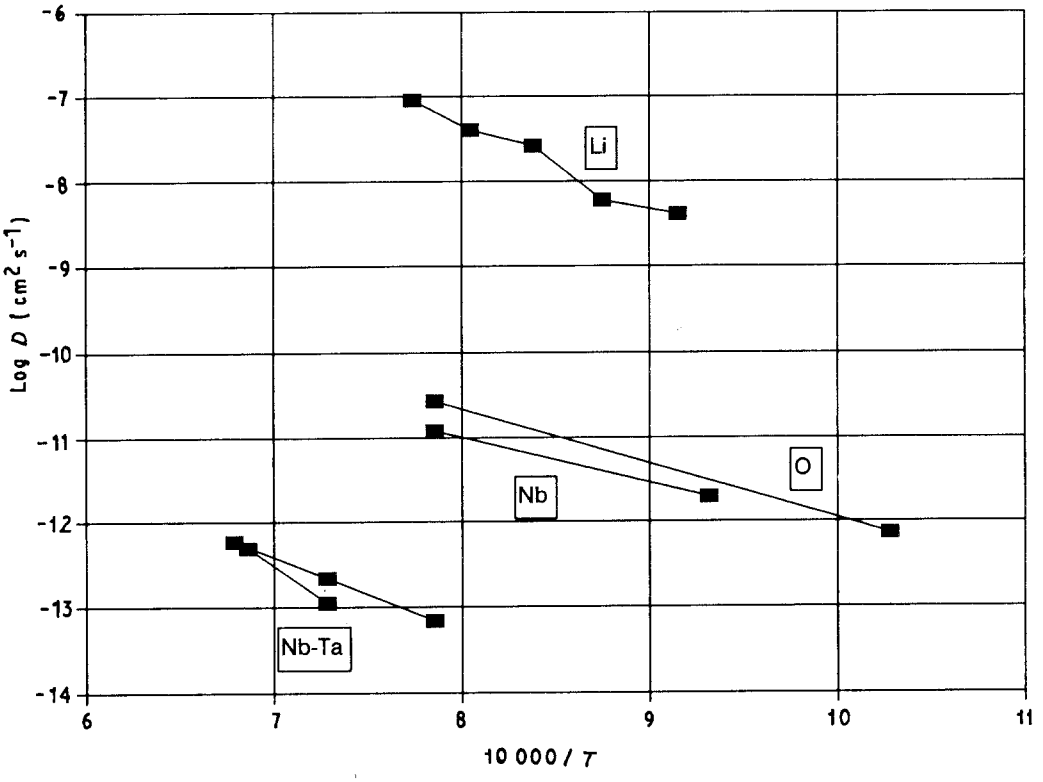

Figure 7 Self diffusion data in lithium niobate. The lithium tracer diffusion data from Fig. 5 are redrawn for comparison with other host-ion diffusion rates.

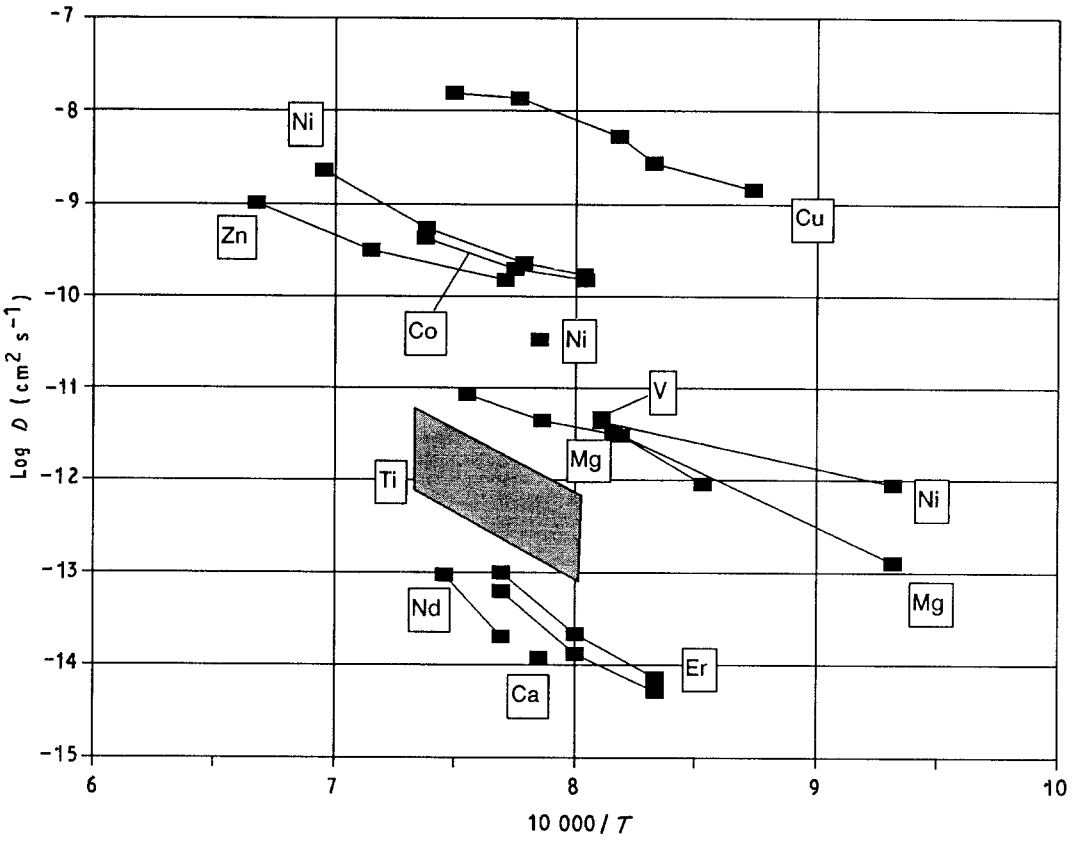

Figure 8 Cation diffusion data. The range of titanium diffusion rates are represented by the shaded region.

TABLE V Cation diffusion in lithium niobate (excluding titanium data)

Atom	Method	T (K)	E_a	D_0 (cm^2 s^{-1})	Comments	References
Mg	EPMA	1173–1323	1.87	1.2×10^{-4}	Y	[68]
Mg	Ion microanalysis	1073–1225	2.43	3.3×10^{-2}	Z	[69]
Cu	WG	1144–1335	1.77	8.5×10^{-2}	$^{\perp}Z$	[70]
Co	WG	1244–1355	1.39	5.9×10^{-5}	$^{\perp}Z$	[70]
Zn	WG	1298–1498	1.59	2.1×10^{-4}	$^{\perp}Z$	[70]
Ni	WG	1244–1438	2.08	3.8×10^{-2}	$^{\perp}Z$	[70]
Ni	Index	1273	–	3.3×10^{-11}	Y	[71]
Ni	WG	1073–1233	1.12	1.7×10^{-7}	Y	[72]
V	WG	1233	–	4.7×10^{-12}	Y	[72]
Er	RBS	1200–1300 1200–1300	3.53 3.36	4.2×10^{0} 5.7×10^{-1}	Z X	[73]
Nd	RBS	1300–1345	5.54	6.1×10^{7}	Z	[73]
Ca	SIMS	1273	–	1.2×10^{-14}	–	[74]

show significantly isotropic behaviour. Larger ions seem to diffuse slower and have somewhat larger activation energies. None of these studies gives any clear information about composition dependence for the diffusion rate; most studies have been performed on samples that probably have the congruent composition.

Fig. 9 shows the compiled titanium diffusion rates. This cluttered figure is a result of numerous studies of optical waveguide formation using titanium in-diffusion. The numerical values are collected in Table VI, with "WG" indicating studies on optical waveguides formed by in-diffusion. The rather wide range of diffusion rates is not unusual when comparing studies performed by different research groups; a number of parameters may influence the wide variation in observed diffusion rates. In the present case the most significant variable may be the base crystal stoichiometry. Because it has taken some time for the true congruent composition to be ascertained, different supplies of crystals have had composition variations with position or between boules [62, 91]; this may have introduced scatter to different researcher's results. Individual plots will be more

TABLE VI Titanium diffusion in lithium niobate

Method	T (K)	E_a	D_0 ($cm^2 s^{-1}$)	Comments	References
EPMA	1273–1373	2.16	1.9×10^{-4}	Y	[45]
WG	1323	–	1.6×10^{-12}	Z, pure	[75]
	1323	–	1.1×10^{-12}	Y, pure	
	1323	–	5.3×10^{-13}	X, Mg-doped	
				$D_Z > D_Y$	
				Mg slows D_{Ti}	
WG	1323	–	5.5×10^{-13}	X, Mg-doped	[76]
EPMA	1273–1373	2.75	2.1×10^{-2}	Y	[41]
EPMA	1323	–	0.4×10^{-12}	50% Li	[77]
	1323	–	1.0×10^{-12}	48.55% Li	
	1323	–	1.5×10^{-12}	48.3% Li	
	1323	–	2.2×10^{-12}	48.1% Li	
WG	1233	–	2.1×10^{-12}	–	[72]
SIMS	1253–1343	3.08	6.8×10^{-1}	Y	[42]
WG	1273–1373	2.49	6.9×10^{-3}	Y	[78]
	1273	–	1.4×10^{-12}	Z	
				$D_Z > D_Y$	
WG	1273	–	6.0×10^{-13}	Isotropic	[79]
WG	1273–1373	3.74	5.2×10^{1}	Mg-doped	[80]
	1323–1373	2.62	1.2×10^{-2}	Pure	
				Mg slows D_{Ti}	
WG	1273	–	1.2×10^{-12}	Wet O_2	[81]
	1273	–	2.6×10^{-12}	Dry O_2	
SIMS	1273	–	6.5×10^{-13}	Y	[82]
WG	1273	–	5.7×10^{-13}	D_Y	[83]
	1273	–	7.9×10^{-13}	D_Z	
				$D_Z > D_Y$	
WG	1273	–	1.5×10^{-12}	D_Y	[84]
	1273	–	1.7×10^{-12}	D_Z	
				$D_Z > D_Y$	
WG	1273–1373	2.44	2.7×10^{-3}	Y	[85]
	1273–1373	2.99	5.4×10^{-1}	Z	
				$D_Z > D_Y$	
WG	1323–1373	2.93	1.2×10^{-1}	X, dry, ext	[86]
	1323–1373	2.58	1.1×10^{-2}	X, dry, ord	
	1323–1373	2.40	2.0×10^{-3}	X, wet, ext	
	1323–1373	2.65	2.2×10^{-2}	X, wet, ord	
	1348–1373	2.45	1.7×10^{-3}	Y, dry, ext	
	1323–1373	2.20	4.1×10^{-4}	Y, dry, ord	
	1348–1373	2.31	9.0×10^{-4}	Y, wet, ext	
	1323–1373	1.85	2.4×10^{-5}	Y, wet, ord	
	1323–1373	1.86	1.7×10^{-5}	Z, dry, ext	
	1323–1373	2.43	3.2×10^{-3}	Z, dry, ord	
	1323–1373	2.53	8.5×10^{-3}	Z, wet, ext	
	1323–1373	2.34	2.2×10^{-3}	Z, wet, ord	
				$D_{wet} > D_{dry}$	
				$D_{ord} > D_{ext}$	
				$D_Z > D_{(X \text{ or } Y)}$	
WG	1244–1345	2.58	3.0×10^{-2}	Y	[87]
WG	1373	–	5.0×10^{-12}	X	[88]
WG	1273	–	7.7×10^{-13}	Y	[89]
	1273		7.1×10^{-13}	Z	
SIMS	1272	–	5.3×10^{-13}	Y	[90]
WG	1273	–	4.6×10^{-13}	Y	[44]

self-consistent when measuring samples from the same batch. Another factor that may have influenced differences in rate from different processes is the diffusion atmosphere. Few systematic studies have been performed, but one comparison gives diffusion rates that are faster when water vapour is included in the atmosphere during annealing [86]. Also, many studies are complicated by performing diffusion in reducing environments (e.g. argon) and then admitting oxygen gas during the cooling down procedure. The effect of these procedures on the diffusion rate is unknown.

Many studies observe slight differences between the diffusion rate parallel (Z-cut) and perpendicular (X- or Y-cut) to the c-axis, with D_Z being slightly faster.

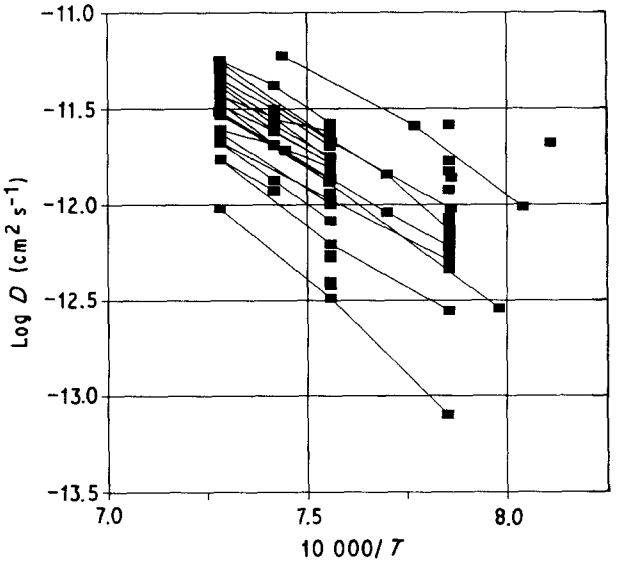

Figure 9 Titanium diffusion data. This ion has been used extensively for making optical waveguide devices. Therefore, plentiful data for this species are available.

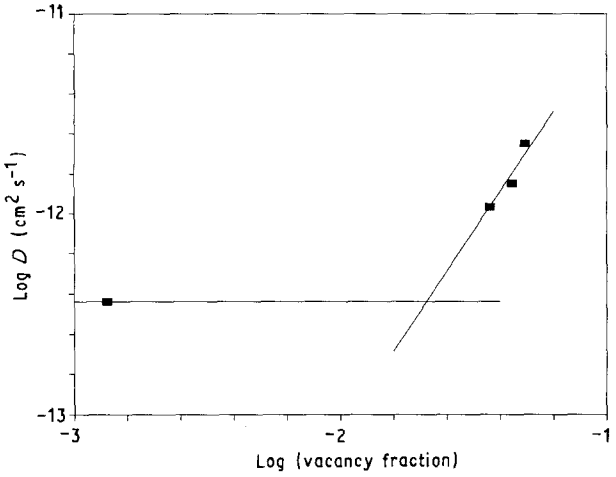

Figure 10 Titanium diffusion rate as a function of cation vacancy fraction, from [77, 91]. This log–log plot illustrates that the data can be represented by a constant component superimposed on a component that varies as the square of the cation vacancy fraction.

However, the difference is small enough that several workers have labelled the diffusion as isotropic. These studies are indicated in the "comments" column of Table VI.

Titanium diffusion appears to be uniformly increased when more cation vacancies are present. This is true for crystals that have different Li/Nb ratios [77, 91] as well as for crystals that have altered cation vacancy concentrations because of doping with aliovalent ions [75, 80]. This behaviour will be the focus for part of the following discussion section.

4. Discussion

One common factor for diffusion of all types of species is that diffusion is very close to isotropic. This is true for hydrogen, lithium, oxygen, titanium, magnesium, and erbium. This is compatible with the crystal structure description given above and the probable migration pathway for ions (on either lithium or niobium sublattice). Thus, the close-packed nature of the oxygen sublattice forces the diffusion to be largely isotropic.

The composition dependence of the titanium diffusion [77, 91] can be analysed using the diffusion equations presented in the first section. The titanium atoms are thought to substitute for niobium atoms [45, 92]. Thus, Equation 19 or 20 must be used to describe diffusion. This equation supports the general composition dependence found above; larger concentrations of cation vacancies increase the diffusion rate. This increase should follow a squared concentration dependence. This should be evident if we plot the logarithm of the diffusion rate versus the logarithm of the cation vacancy concentration. Fig. 10 gives this plot. The points taken at larger deviation from stoichiometry can be represented as a line with slope of 2, whereas there is a background level that would represent a constant diffusivity in nearly stoichiometric material. These contributions come from diffusion on the two separate sublattices.

The apparent contributions from two different mechanisms emphasizes the importance of site swapping for impurities in lithium niobate. This is compatible with other work where site-fraction changes with temperature has been observed [31, 33]. It may also help to explain the relative difficulty of assigning impurity substitution sites. Future work should carefully include dynamic site swapping in making defect-site assessments.

5. Conlusion

The defect chemistry of non-stoichiometry and impurity incorporation in lithium niobate has been reviewed. The important aspect of cation sublattice swapping has been factored into a description of different diffusion paths. It was found that impurities that substitute primarily for niobium could be migrating chiefly on the lithium sublattice. Titanium diffusion data seem to exhibit this behaviour.

Overall, the review of diffusion data emphasizes the relatively isotropic nature of diffusion in this structure. This behaviour can be understood upon close examination of the crystal structure and available pathways through the close-packed oxygen lattice.

Acknowledgements

The author thanks Peter Bordui and Gary Catchen who happily provided copies of their pre-publication manuscripts.

References

1. M. M. ABOUELLEIL and F. J. LEONBERGER, *J. Amer. Ceram. Soc.* **72** (1989) 1311.
2. R. S. WEIS and T. K. GAYLORD, *Appl. Phys.* **A37** (1985) 191.
3. C. S. TSAI, *Jpn J. Appl. Phys.* **19** (Suppl. 1) (1980) 661.
4. S. C. ABRAHAMS, J. M. REDDY and J. L. BERNSTEIN, *J. Phys. Chem. Solids* **27** (1966) 997.
5. S. C. ABRAHAMS, W. C. HAMILTON and J. M. REDDY, *ibid.* **27** (1966) 1013–18.

6. S. C. ABRAHAMS, H. J. LEVINSTEIN and J. M. REDDY, *ibid.* **27** (1966) 1019.
7. W. D. JOHNSTON and I. P. KAMINOW, *Phys. Rev.* **168** (1968) 1045.
8. R. C. MILLER and A. SAVAGE, *Appl. Phys. Lett.* **9** (1966) 169.
9. D. P. BIRNIE III, *J. Mater. Res.* **5** (1990) 1933.
10. *Idem, J. Amer. Ceram. Soc.* **74** (1991) 988.
11. P. LERNER, C. LEGRAS and J. P. DUGAS, *J. Crystal Growth* **3** (1968) 231.
12. G. E. PETERSON, and J. R. CARRUTHERS, *J. Solid State Chem.* **1** (1969) 98.
13. G. E. PETERSON and A. CARNAVALE, *J. Chem. Phys.* **56** (1972) 4848.
14. S. C. ABRAHAMS and P. MARSH, *Acta Crystallogr.* **B42** (1986) 61.
15. L. KOVACS and K. POLGAR, *Cryst. Res. Technol.* **21** (1986) K101.
16. Y. LIMB, K. W. CHENG and D. M. SMYTH, *Ferroelect.* **38** (1981) 813.
17. D. M. SMYTH, *ibid.* **50** (1983) 93.
18. *Idem,* in Proceedings of the 6th IEEE International Symposium on Application of Ferroelectrics", Bethlehem, PA (1986) pp. 115–17.
19. E. K. CHANG, A. MEHTA and D. M. SMYTH, *Adv. Ceram.* **23** (1987) 351.
20. A. MEHTA, E. K. CHANG and D. M. SMYTH, *J. Mater. Res.* **6** (1991) 851.
21. F. A. KRÖGER, "The Chemistry of Imperfect Crystals" (North Holland, Amsterdam, 1964).
22. P. K. GALLAGHER and H. M. O'BRYAN, *J. Amer. Ceram. Soc.* **71** (1988) C 56.
23. K. L. SWEENEY and L. E. HALLIBURTON, *Appl. Phys. Lett.* **43** (1983) 336.
24. P. J. JORGENSEN and R. W. BARTLETT, *J. Phys. Chem. Solids* **30** (1969) 2639.
25. S. G. BOYER and D. P. BIRNIE III, in "Proceedings SPIE 968", "Ceramics and Inorganic Crystals for Optics, Electro-Optics, and Nonlinear Conversion" (1988) p. 73.
26. D. G. REXFORD, Y. M. KIM and H. S. STORY, *J. Chem. Phys.* **52** (1970) 860.
27. H. H. TOWNER, Y. M. KIM and H. S. STORY, *ibid.* **56** (1972) 3676.
28. P. F. McDONALD, C. P. TAM and Y. W. MOK, *ibid.* **56** (1972) 1007.
29. A. A. KAMINSKII, *Sov. Phys. Cryst.* **17** (1972) 194.
30. L. REBOUTA, J. C. SOARES, M. F. da SILVA, J. A. SANZ-GARCIA, E. DIEGUEZ and F. AGULLO-LOPEZ, *Appl. Phys. Lett.* **55** (1989) 120.
31. T. TOMOV, H. ENGELMANN, I. DEZSI and U. GONSER, *Solid. State Commun.* **69** (1989) 41.
32. P. W. HAYCOCK and P. D. TOWNSEND, *Rad. Effects* **98** (1986) 243.
33. G. L. CATCHEN, J. M. ADAMS and T. M. REARICK, *Phys. Rev. B* **46** (1992) 2743.
34. C. P. MARSHALL and W. A. DOLLASE, *Amer. Mineral.* **69** (1984) 928.
35. D. P. BIRNIE III, *J. Phys. Chem. Solids* **51** (1990) 1313.
36. *Idem, J. Amer. Ceram. Soc. Commun.* **69** (1986) c33.
37. *Idem, J. Amer. Ceram. Soc.* **72** (1989) 1277.
38. P. G. SHEWMON, "Diffusion in Solids", (McGraw-Hill, New York, 1963).
39. R. J. BORG and G. J. DIENES, "An Introduction to Solid State Diffusion" (Academic Press, San Diego, 1988).
40. C. E. RICE, J. L. JACKEL and W. L. BROWN, *J. Appl. Phys.* **57** (1985) 4437.
41. M. MINAKATA, S. SAITO, M. SHIBATA and S. MIYAZAWA, *J. Appl. Phys.* **49** (1978) 4677.
42. R. A. BETTS, C. W. PITT, K. R. RIDDLE and L. M. WALPITA, *Appl. Phys. A* **31** (1983) 29.
43. S. FRIES, P. HERTEL and H. P. MENZLER, *Phys. Status Solidi* **A108** (1988) 449.
44. J. VOLLMER, J. P. NISIUS, P. HERTEL and E. KRÄTZIG, *Appl. Phys.* **A32** (1983) 125.
45. K. SUGII, M. FUKUMA and H. IWASAKI, *J. Mater. Sci.* **13** (1978) 523.
46. C. CANALI, A. CARNERA, G. DELLA MEA, P. MAZZOLDI, S. M. AL SHUKRI, A. C. G. NUTT and R. M. De La RUE, *J. Appl. Phys.* **59** (1986) 2643. (Replotted with additional factor of 4 to conform to common diffusion constant practice.)
47. R. GONZALEZ, Y. CHEN, K. L. TSANG and G. P. SUMMERS, *Appl. Phys. Lett.* **41** (1982) 739.
48. A. LONI, R. M. De La RUE and J. M. WINFIELD, *J. Appl. Phys.* **61** (1987) 64.
49. J. L. JACKEL, C. E. RICE and J. J. VESELKA, *Ferroelectrics* **50** (1983) 165.
50. D. F. CLARK, A. C. G. NUTT, K.K. WONG, P. J. R. LAYBOURN and R. M. De La RUE, *J. Appl. Phys.* **54** (1983) 6218.
51. K. K. WONG, A. C. G. NUTT. D. F. CLARK, J. WINFIELD, P. J. R. LAYBOURN and R. M. De La RUE, *IEE Proc. J* **133** (2) (1986) 113.
52. M. GOODWIN and C. STEWART, *Elecron. Lett.* **19** (1983) 223.
53. C. WARREN, S. FOROUHAR, W. S. C. CHANG and S. K. YAO, *Appl. Phys. Lett.* **43** (1983) 424.
54. M. DIGONNET, M. FEJER and R. BYER, *Opt. Lett.* **10** (1985) 235.
55. J. R. CARRUTHERS, I. P. KAMINOW and L. W. STULZ, *Appl. Opt.* **13** (1974) 2333.
56. I. P. KAMINOW and J. R. CARRUTHERS, *Appl. Phys. Lett.* **22** (1973) 326.
57. A. MEHTA, E. K. CHANG and D. M. SMYTH, *J. Mater. Res.* **6** (1991) 851.
58. T. K. HALSTEAD, *J. Chem. Phys.* **53** (1970) 3427.
59. V. E. WOOD, N. F. HARTMAN, A. E. AUSTIN and C. M. VERBER, *J. Appl. Phys.* **52** (1981) 1118.
60. V. B. PTASHNIK, T. Y. DUNAEVA and I. V. MYASNIKOV, *Inorg. Mater.* **21** (1985) 1814.
61. N. SCHMIDT, K. BETZLER, M. GRABS, S. KAPPHAN and F. KLOSE, *J. Appl. Phys.* **65** (1989) 1253.
62. R. L. HOLMAN, *Mater. Sci. Res.* **11** (1978) 343.
63. D. H. JUNDT, M. M. FEJER, R. G. NORWOOD and P. F. BORDUI, *J. Appl. Phys.* (1992) submitted.
64. V. I. LAPSHIN and A. P. RUMYANTSEV, *Inorg. Mater.* **12** (1976) 1797.
65. G. Y. CHIN, A. A. BALLMAN, P. K. TIEN and S. RIVA SANSEVERINO, *Appl. Phys. Lett.* **26** (1975) 637.
66. W. PHILLIPS and J. M. HAMMER, *J. Electron. Mater.* **4** (1975) 549.
67. B. DISCHLER, J. R. HERRINGTON, A. RAÜBER and H. KURZ, *Solid State Commun.* **14** (1974) 1233.
68. J. NODA, M. FUKUMA and S. SAITO, *J. Appl. Phys.* **49** (1978) 2150.
69. K. KOMATSU, M. KONDO and Y. OHTA, *Electron. Lett.* **22** (1986) 881.
70. G. D. BOYD, R. V. SCHMIDT and F. G. STORZ, *J. Appl. Phys.* **48** (1977) 2880.
71. J. M. WHITE and P. F. HEIDRICH, *Appl. Opt.* **15** (1976) 151.
72. R. V. SCHMIDT and I. P. KAMINOW, *Appl. Phys. Lett.* **25** (1974) 458.
73. C. BUCHAL and S. MOHR, *J. Mater. Res.* **6** (1991) 134.
74. D. LANDHEER, D. F. MITCHELL and G. I. SPROULE, *J. Vac. Sci. Technol. A* **4** (1986) 1897.
75. G. ARVIDSSON, A. SJÖBERG, A. A. LIPOVSKY and F. LAURELL, in Technical Digest, "1986 Conference on Lasers and Electro-optics" (CLEO '86), San Francisco, 9–13 June 1986, p. 228.
76. A. SJÖBERG, G. ARVIDSSON and A. A. LIPOVSKII, *J. Opt. Soc. Amer. B* **5** (1988) 285.
77. R. J. HOLMES and D. M. SMYTH, *J. Appl. Phys.* **55** (1984) 3531.
78. W. K. BURNS, P. H. KLEIN, E. J. WEST and L. E. PLEW, *J. Appl. Phys.* **50** (1979) 6175.
79. C. CANALI, C. de BERNARDI, M. de SARIO, A. LOFFREDO, G. MAZZI and S. MORASCA, *J. Lightwave Technol.* **LT-4** (1986) 951.

80. C. H. BULMER, *Electron. Lett.* **20** (1984) 902.
81. M. VALLI, A. FIORETTI and M. N. ARMENISE, *J. Mod. Opt.* **35** (1988) 885.
82. T. BREMER, P. HERTEL, S. OELSCHIG, R. SOMMERFELDT and W. HEILAND, *Thin Solid Films* **175** (1989) 235.
83. L. TSONEV, I. SAVATINOVA and P. SIMOVA, *Appl. Phys.* **24** (1981) 205.
84. J. CTYROKY, M. HOFMAN, J. JANTA and J. SCHRÖFEL, *IEEE J. Quant. Electron.* **QE-20** (1984) 400.
85. M. FUKUMA and J. NODA, *Appl. Opt.* **19** (1980) 591.
86. O. EKNOYAN, A. S. GREENBLATT, W. K. BURNS and C. H. BULMER, *ibid.* **25** (1986) 737.
87. H. NAITOH, M. NUNOSHITA and T. NAKAYAMA, **16** (1977) 2546.
88. J. F. WELLER, J. D. CROWLEY and T. G. GIALLORENZI, *Appl. Phys. Lett.* **31** (1977) 146.
89. M. FUKUMA, J. NODA and H. IWASAKI, *J. Appl. Phys.* **49** (1978) 3693.
90. T. BREMER, D. KOLLEWE, H. KOSCHMIEDER and W. HEILAND, *Fresenius Z. Anal. Chem.* **333** (1989) 485.
91. R. J. HOLMES and W. J. MINFORD, *Ferroelect.* **75** (1987) 63.
92. C. BUCHAL and S. MANTL, *Mater. Res. Soc. Symp. Proc.* **100** (1988) 317.

Received and accepted 14 May 1992